State of Charge Imbalance Estimation for Battery Strings Under Reduced Voltage Sensing

Xinfan Lin, Anna G. Stefanopoulou, *Fellow, IEEE*, Yonghua Li, and R. Dyche Anderson

***Abstract*— Reducing voltage sensing in a battery pack is beneficial for cutting the cost of the battery management system. In this paper, a methodology is designed to estimate the states of charge (SOC) of two cells connected in series when only their total voltage is measured. First, the feasibility is analyzed based on the nonlinear observability of the two-cell string under reduced voltage sensing. Furthermore, observability analysis is performed to different battery chemistries to determine their respective observable SOC ranges based on the voltage-SOC relationship. A trajectory-based nonlinear observer, the Newton observer, is then designed for SOC estimation and has been validated by experiments. The limitation of extending the method to strings with more than two cells is also discussed. The methodology is initially designed under the assumption of equal and known capacity and resistance among cells. The robustness of estimation is finally investigated when the above assumptions do not hold.**

***Index Terms*— Battery control, observability, reduced voltage sensing, state estimation.**

I. Introduction

BATTERY pack, as a common energy storage system, are a major component of most electric vehicles (EV). Among all types of batteries, lithium-ion batteries are nowadays widely used for automotive applications. Compared with other battery chemistries, such as lead-acid and nickel-metal hydride (NiMH), lithium-ion batteries have advantages in the following aspects [1]–[5]:

1) high energy density (>150 Wh/kg);
2) high open circuit voltage (OCV) (>3.2 V, high power);
3) long cycle life;
4) high charge efficiency (97%–99%);
5) no memory effect.

Lithium-ion batteries do have weaknesses, especially a vulnerability to overcharge and overdischarge. Overcharge might lead to lithium deposition and electrolyte solvent decomposition, resulting in fire or even explosion [5]–[7]. This issue is especially critical for battery packs in plug-in hybrid EV (PHEV) and battery EV (BEV), since those batteries are usually charged to high states of charge (SOC). Overdischarge will potentially damage the cell by causing copper dissolution and dendrite formation [6], [7]. Primarily to prevent overcharge, for lithium-ion batteries connected in series, the voltage of every cell is monitored. This single cell voltage monitoring scheme is referred to as the full voltage sensing. Current practice for lead-acid and NiMH batteries is to measure the voltage at 5–12 cell intervals, due to their higher tolerance to overcharge. Such voltage monitoring scheme is referred to as the reduced voltage sensing.

Full voltage sensing adds to the cost and complexity of the battery management system. The EV battery packs often contain hundreds or even thousands of cells. To implement full voltage sensing, each cell or combination of parallel cells must be monitored. This requires a substantial number of sensing leads, sensors, wiring, and labor. System reliability is negatively impacted due to the high number of parts. Furthermore, it also requires significant computation and data storage capacity for the BMS to process the single-cell voltage measurement for monitoring or SOC estimation. All these complexities create significant incentives to replace full voltage sensing with reduced voltage sensing.

The reduced voltage sensing must retain the ability to prevent overcharge and overdischarge of all cells. Prior art for preventing or detecting overcharge and/or overdischarge in a reduced voltage sensing environment (such as those used with lead-acid or NiMH batteries) involves treating the cells in a given module as identical, and the voltage of a single cell can be obtained by dividing the total voltage by the number of cells in series. When the cell SOCs and voltages are unbalanced, however, the voltage of a single cell cannot be inferred from the total voltage.

The SOC imbalance is present in all large battery packs, and it can be caused by a number of factors, including manufacturing variability, differing self-discharge rates, and varying rates of capacity change over life [8]–[10]. Furthermore, two cells that are at the same SOC can be at different voltages (under load) if their internal resistances are different. The SOC imbalance reduces the available energy in a pack, decreasing electric range to PHEV and BEV customers. A small amount of SOC imbalance is of less concern in HEV batteries, since less of the full SOC operating range is typically used, but even in HEVs if imbalance grows too high the available charge and/or discharge power to the vehicle is reduced.

Manuscript received December 11, 2013; revised July 7, 2014 and September 7, 2014; accepted September 14, 2014. Date of publication November 20, 2014; date of current version April 14, 2015. Manuscript received in final form September 22, 2014. Recommended by Associate Editor S. Varigonda.

X. Lin is with the Department of Mechanical Engineering, University of Michigan, Ann Arbor, MI 48109 USA, and also with the Department of Vehicle Controls and Systems Engineering, Ford Research and Advanced Engineering, Ford Motor Company, Dearborn, MI 48124 USA (e-mail: xflin@umich.edu).

A. G. Stefanopoulou is with the Department of Mechanical Engineering, University of Michigan, Ann Arbor, MI 48109 USA (e-mail: annastef@umich.edu).

Y. Li is with Global Powertrain Controls and System Engineering, Ford Motor Company, Dearborn, MI 48124 USA (e-mail: yli19@ford.com).

R. D. Anderson is with the Department of Vehicle Controls and Systems Engineering, Ford Research and Advanced Engineering, Ford Motor Company, Dearborn, MI 48121 USA (e-mail: rander34@ford.com).

Color versions of one or more of the figures in this paper are available online at http://ieeexplore.ieee.org.

Digital Object Identifier 10.1109/TCST.2014.2360919

Due to the common presence of SOC imbalance among cells, to avoid cell overcharge/overdischarge under reduced voltage sensing, the individual cell SOCs and voltages need to be estimated based on the total voltage. The SOC estimation has been well studied under full voltage sensing, but barely under reduced sensing. The proposed methods in literature include Coulomb counting [11], Luenberger observer [12], [13], extended Kalman filter (EKF) [14], [15], unscented Kalman filter [13], [16], sliding mode observer [17] among others. The algorithms are usually applied to estimate the SOC of single cells using their own voltage measurement. Recently, there have been attempts to improve the SOC estimation by analyzing the difference between individual cell voltages (or between individual and average) in a series battery string, such as [18] and [19]. These methods, however, still rely on measurement of single cell voltage. Estimation under reduced voltage sensing has been attempted in [20], where the single cell voltage is estimated based on the instantaneous change in total voltage before and after the balancing circuit is switched. The accuracy of the estimation, however, is compromised by the high ratio of the bypass resistance to the cell internal resistance. The method in [20] also requires manipulation of the balancing circuit.

In this paper, the estimation of individual cell SOCs and voltages will be addressed solely based on the total voltage of cells connected in series. The basic idea is first introduced in Section II, where it is shown that the cell SOCs are observable from the trajectory of the total voltage over time given a known nonlinear voltage versus SOC relationship. The observability depends on the cell chemistry and other factors. The estimation problem is then formulated mathematically in Section III based on defined assumptions and conditions. In Section IV, observability analysis is conducted to derive the necessary conditions for solving the estimation problem. In Section V, a trajectory-based nonlinear observer, the Newton observer, is designed and validated by experiments. Finally, the robustness of the estimation under model uncertainty is analyzed in Section VI.

II. Basic Idea

In this section, it will be shown intuitively that the individual cell SOCs are observable from the trajectory of the total voltage over time if the battery voltage versus SOC relationship is nonlinear.

As an example for illustration, the voltage versus SOC relationship of a lithium iron phosphate ($LiFePO_4$) battery under a constant charging current is shown in Fig. 1. Assume at time $t = 0$ s, a total voltage of 6.88 V is measured across a two-cell string, there would be infinite combinations of individual cell SOCs giving this total voltage. Three of such combinations are given in Table I, and shown in the inset of Fig. 1. It is not possible to distinguish these combinations based on the total voltage measurement at a single time instant. The SOC combinations are, however, distinguishable based on the trajectory of the total voltage over time. Under the constant charging current, trajectories of the total voltage over time in the three cases are shown in Fig. 2.

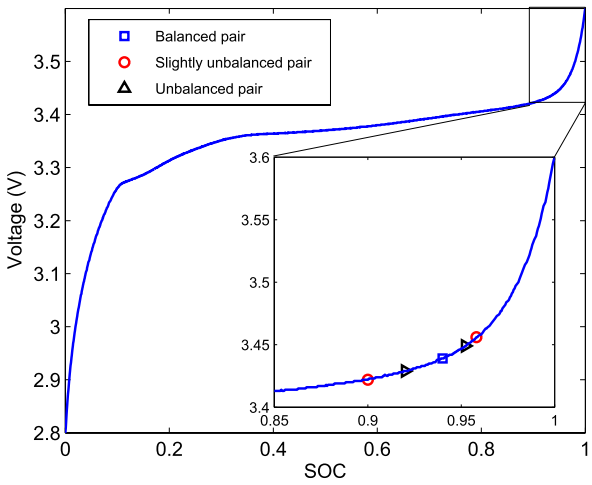

Fig. 1. Voltage versus SOC relationship of a $LiFePO_4$ battery under a constant charging current. Inset: three SOC combinations giving the same total voltage as listed in Table I.

TABLE I
SOC Combinations Giving the Same Total Voltage Instantaneously

	SOC_1	SOC_2	Total Voltage (V)
Balanced Pair	0.94	0.94	6.88
Slightly Unbalanced Pair	0.95	0.92	6.88
Unbalanced Pair	0.96	0.90	6.88

It can be seen that due to the nonlinearity of the voltage versus SOC relationship, the three trajectories are different. The main idea of this paper is to estimate the single cell SOCs and voltages based on the trajectory of the total voltage over time.

III. Problem Formulation

In this paper, the SOC estimation problem under reduced voltage sensing is analyzed under the following assumptions and conditions.

1) Most of the analysis is conducted for reduced voltage sensing, which measures two cell intervals, targeting 50% reduction in voltage sensing in a battery pack. The methodology can be extended to longer intervals but is subject to practical limitation to be discussed in Section IV.
2) The method is first designed to estimate SOCs under the assumption that capacity and resistance are known and equal among cells. Possible cause of SOC imbalance under such circumstance is the difference among cells in self-discharge rate.
3) In reality, SOC imbalance can also be induced by varying capacity (or capacity fading rate) among cells. The developed method will be applied for SOC estimation under such circumstance in Section VI. In this case, SOC estimation will likely be affected by model uncertainty, which is the mismatch between the rated and the (unknown) actual capacity and resistance. The SOC estimation error under such circumstance will be quantified.

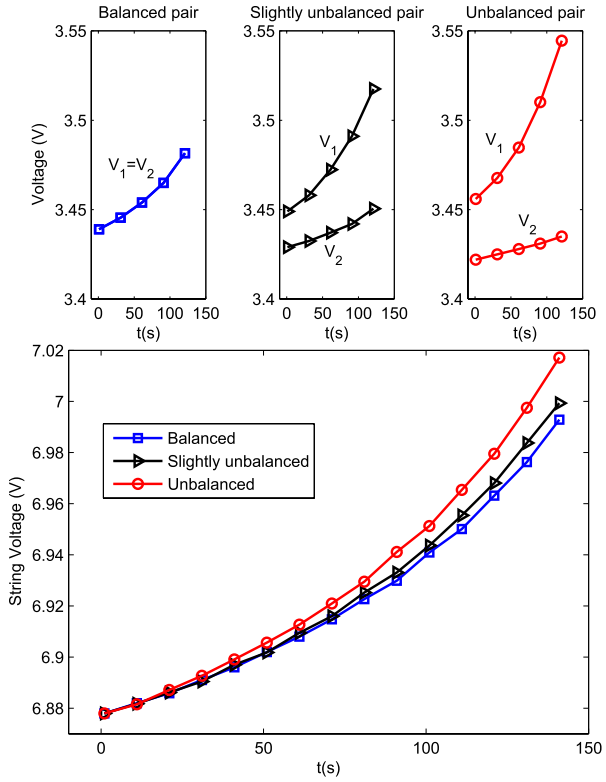

Fig. 2. Voltage trajectory over time under a constant charging current of the three SOC combinations in Table I. Three subplots on the top: trajectory of the individual cell voltages of each combination. Bottom subplot: trajectories of the three total voltages.

4) The operating condition is constant current (CC) charging, where a coulomb counting model is sufficient to capture the voltage dynamics. The capability of imbalance estimation under CC charging is important for the following two reasons. First, knowledge of the SOC imbalance during charging is critical to avoid overcharging the cell with higher SOC, especially when the cell SOCs are high at the end of charging. Second, charging is also usually the (best) timing to perform cell balancing, and knowledge of the SOC imbalance needs to be used for guidance. It is possible to apply the designed algorithm to real-world driving conditions with more complicated and accurate dynamic battery models.

The Coulomb counting model for the battery voltage response used in this paper takes the form

$$\begin{aligned} x_{k+1} &= x_k + \frac{I\Delta t}{Q} \\ V_k &= g(x_k) + IR \end{aligned} \tag{1}$$

where x is the SOC, V is the voltage, Δt is the sampling period, I is the current (positive for charging), Q is the battery capacity, and R is the ohmic resistance.

The term $g(x)$ is a nonlinear relationship between battery voltage and SOC under the constant charging current, which may include the OCV, hysteresis voltage, and polarization over-potential among others. If the estimation is to be extended to dynamic drive cycles in future, more complicated models such as the equivalent circuit model including parallel R–C pairs or single particle model capturing lithium intercalation [21]–[23] need to be considered. Consider a battery string with two cells connected in series, the string model can be written as

$$\begin{aligned} x_{\text{str},k} &= \begin{bmatrix} x_{1,k} & x_{2,k} \end{bmatrix}^T \\ x_{\text{str},k+1} &= \begin{bmatrix} x_{1,k+1} \\ x_{2,k+1} \end{bmatrix} = \begin{bmatrix} x_{1,k} + \frac{I\Delta t}{Q} \\ x_{2,k} + \frac{I\Delta t}{Q} \end{bmatrix} \\ V_{\text{str},k} &= V_{1,k} + V_{2,k} = g(x_{1,k}) + g(x_{2,k}) + 2IR \end{aligned} \tag{2}$$

where subscripts 1 and 2 are used to denote the variables associated with cell 1 and 2. The goal of estimation is to determine $x_{1,k}$ and $x_{2,k}$ when I is known and V_{str} is measured over a period of time.

IV. Observability Analysis

In this section, the observability of the individual cell SOCs under reduced voltage sensing is investigated. The derived observability condition is shown to be dependent on the nonlinearity of the voltage-SOC relationship. Extension to general cases (n cell intervals) is also discussed.

A. Observability Matrix of a Two-Cell Battery String

Starting from time step k, the trajectory of the total voltage V_{str} over $N+1$ consecutive time steps $k, k+1, \ldots, k+N$, $V_{\text{str},[k,k+N]}$, can be denoted as

$$\begin{aligned} V_{\text{str},[k,k+N]} &= \begin{bmatrix} V_{\text{str},k} \\ V_{\text{str},k+1} \\ \cdots \\ V_{\text{str},k+N} \end{bmatrix} \\ &= \begin{bmatrix} g(x_{1,k}) + g(x_{2,k}) + 2IR \\ g(x_{1,k+1}) + g(x_{2,k+1}) + 2IR \\ \cdots \\ g(x_{1,k+N}) + g(x_{2,k+N}) + 2IR \end{bmatrix}. \end{aligned} \tag{3}$$

Based on the battery string model under CC charging in (2), $V_{\text{str},[k,k+N]}$ can be further written as a function of the initial states, $x_{\text{str},k}$, as

$$\begin{aligned} V_{\text{str},[k,k+N]} &= H(x_{\text{str},k}) \\ &= \begin{bmatrix} g(x_{1,k}) + g(x_{2,k}) + 2IR \\ g\left(x_{1,k} + \frac{I\Delta t}{Q}\right) + g\left(x_{2,k} + \frac{I\Delta t}{Q}\right) + 2IR \\ \cdots \\ g\left(x_{1,k} + \frac{NI\Delta t}{Q}\right) + g\left(x_{2,k} + \frac{NI\Delta t}{Q}\right) + 2IR \end{bmatrix}. \end{aligned} \tag{4}$$

By taking the partial derivative of H to $x_{\text{str},k}$, deviation of the trajectory caused by variation in the initial states can be obtained as

$$\begin{aligned} \delta V_{\text{str},[k,k+N]} &= \frac{\partial H}{\partial x_{\text{str},k}} \delta x_{\text{str},k} \\ &= \begin{bmatrix} g'(x_{1,k}) & g'(x_{2,k}) \\ g'\left(x_{1,k} + \frac{I\Delta t}{Q}\right) & g'\left(x_{2,k} + \frac{I\Delta t}{Q}\right) \\ \cdots & \cdots \\ g'\left(x_{1,k} + \frac{NI\Delta t}{Q}\right) & g'\left(x_{2,k} + \frac{NI\Delta t}{Q}\right) \end{bmatrix} \delta x_{\text{str},k} \end{aligned} \tag{5}$$

where $g'(x)$ denotes the gradient of $g(x)$ to x. In (5), $\delta x_{\text{str},k}$ represents the deviation of initial SOCs from the nominal point, $x^0_{\text{str},k}$, that is, $\delta x_{\text{str},k} = x_{\text{str},k} - x^0_{\text{str},k}$. For example, for the three cases in Table I, if the nominal guess is defined at the balanced combination, $x^0_{\text{str},k} = [0.94, 0.94]^T$, $\delta x_{\text{str},k}$ of the three cases would be

$$\begin{aligned}
&\delta x_{1,k} = \delta x_{2,k} = 0, \quad \text{for balanced pair} \\
&\delta x_{1,k} = -0.02, \quad \delta x_{2,k} = 0.01 \quad \text{for slightly unbalanced pair} \\
&\delta x_{1,k} = -0.04, \quad \delta x_{2,k} = 0.02 \quad \text{for unbalanced pair.}
\end{aligned} \tag{6}$$

Estimating $x_{\text{str},k}$ is equivalent to estimating $\delta x_{\text{str},k}$. In order for $\delta x_{\text{str},k}$ to be observable from $\delta V_{\text{str},[k,k+N]}$, $\partial H/\partial x_{\text{str},k}$ needs to be a one-to-one mapping and hence of full rank (rank = 2). In fact, $\partial H/\partial x_{\text{str},k}$ is by definition the observability matrix of the nonlinear discrete-time system in [24, eq. (2)]

$$O_D(x_{\text{str},k}) = \frac{\partial H}{\partial x_{\text{str},k}}(x_{\text{str},k}). \tag{7}$$

The reason that $x_{\text{str},k}$ cannot be observed from the measurement of $V_{\text{str},k}$ at a single time instant can be found in the observability matrix. With only $V_{\text{str},k}$, (5) is reduced to

$$\delta V_{\text{str},k} = O_D(x_{\text{str},k})\delta x_{\text{str},k} = g'(x_{1,k})g'(x_{2,k})\delta x_{\text{str},k}. \tag{8}$$

The observability matrix only has one row, and thus its rank is one. Rank deficiency indicates that there are infinite numbers of $\delta x_{\text{str},k}$ that could match the single $\delta V_{\text{str},k}$. Only when multiple V_{str} data are processed at the same time, would the $O_D(x_{\text{str},0})$ matrix have more than one rows and hence be possible to have full rank. Still, more rows do not necessarily guarantee observability. For example, when $g(x)$ is linear and $g'(x)$ is constant, additional rows do not make O_D full rank, since the two columns of O_D are identical. Necessary conditions on $g(x)$ for observability will be discussed.

B. Observability Conditions Based on $g(x)$

The discrete-time observability matrix in (5) can be transformed to the continuous-time observability matrix, as

$$O_C(x_{\text{str},k}) = \begin{bmatrix} g'(x_{1,k}) & g'(x_{2,k}) \\ g''(x_{1,k})\frac{I}{Q} & g''(x_{2,k})\frac{I}{Q} \end{bmatrix} \tag{9}$$

where $g''(x)$ denotes the second-order gradient of $g(x)$ to x. This O_C matrix can also be obtained based on the Lie derivatives of the continuous battery string model [25], [26]. The first-order gradient of $g(x)$, $g'(x)$, is usually positive, since the battery voltage normally increases monotonically with SOC. Therefore, for $O_C(x_{\text{str}})$ to be of full rank, it is necessary that either $g''(x_{1,k})$ or $g''(x_{2,k})$ needs to be nonzero, which means that $g(x)$ should be nonlinear. Two lithium-ion battery chemistries are taken as examples for illustration.

The $g(x)$ function of a $LiFePO_4$ battery under 1 C constant charging current is plotted in Fig. 3, along with its first- and second-order gradients. It can be seen that in the middle SOC range, 15%–90%, $g(x)$ is almost linear, with small first- and second-order gradients. As a result, the observability matrix O_C will be practically rank deficient. At the high and low SOC ends, namely, 0%–15% and 90%–100%, $g(x)$ is highly nonlinear with significant $g'(x)$ and $g''(x)$. These regions are

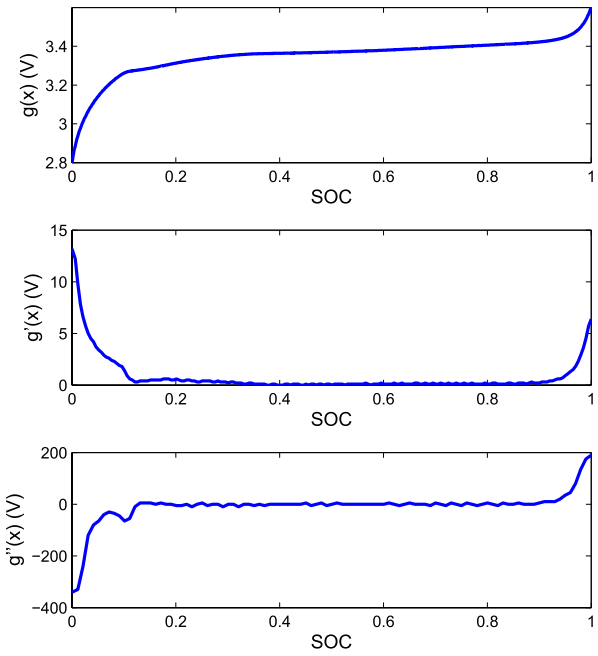

Fig. 3. Voltage function $g(x)$ of a $LiFePO_4$ battery under a constant charging current and its gradients. Top: $g(x)$. Middle: first-order gradient $g'(x)$. Bottom: second-order gradient $g''(x)$.

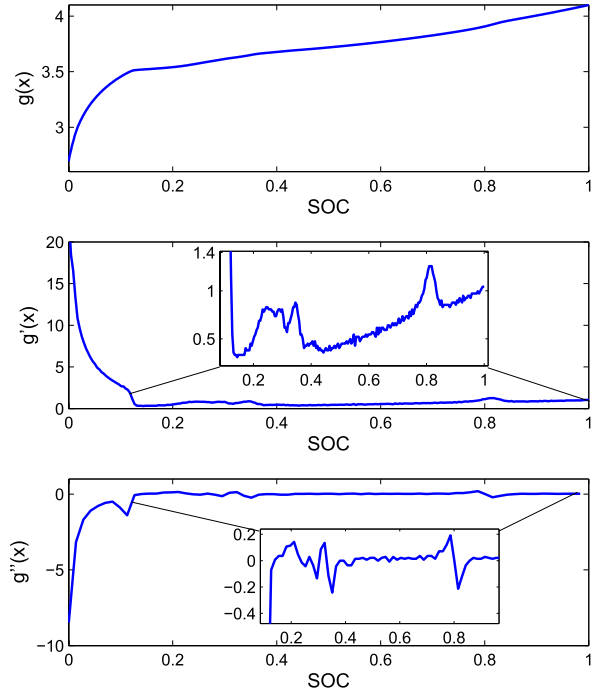

Fig. 4. Voltage function $g(x)$ of a LiNMC battery under a constant charging current and its gradients. Top: $g(x)$. Middle: first-order gradient $g'(x)$. Bottom: second-order gradient $g''(x)$.

where the precaution against overcharge and overdischarge is critically needed. Fortunately, the highly nonlinear $g(x)$ in these ranges renders significant observability to the individual cell SOCs and voltages. It is noted that for the $LiFePO_4$ chemistry, SOC is barely observable in the middle SOC range even under full voltage sensing, due to the flatness of $g(x)$.

As another example, $g(x)$ of a LiNiMnCo (LiNMC) battery and its first- and second-order gradients are shown in Fig. 4.

$$O_C(x_{\mathrm{str},k}) = \begin{bmatrix} g'(x_{1,k}) & g'(x_{2,k}) & \cdots & g'(x_{n,k}) \\ g''(x_{1,k})\frac{I}{Q} & g''(x_{2,k})\frac{I}{Q} & \cdots & g''(x_{n,k})\frac{I}{Q} \\ & \cdots & & \\ g^{(i)}(x_{1,k})\left(\frac{I}{Q}\right)^{i-1} & g^{(i)}(x_{2,k})\left(\frac{I}{Q}\right)^{i-1} & \cdots & g^{(i)}(x_{n,k})\left(\frac{I}{Q}\right)^{i-1} \\ & \cdots & & \\ g^{(n)}(x_{1,k})\left(\frac{I}{Q}\right)^{n-1} & g^{(n)}(x_{2,k})\left(\frac{I}{Q}\right)^{n-1} & \cdots & g^{(n)}(x_{n,k})\left(\frac{I}{Q}\right)^{n-1} \end{bmatrix} \tag{10}$$

For this battery chemistry, the strongly observable SOC range is below 10%, where both $g'(x)$ and $g''(x)$ are large enough. When the SOC is above 10%, linear $g(x)$ [nearly zero $g''(x)$] inhibits the observability under reduced voltage sensing. Slight nonlinearity is noted around 80% SOC, rendering that range weakly observable.

C. Extension to General Cases

When the total voltage is measured for every n cells, $n > 2$, observability analysis can be conducted in a similar way. Using the Lie-derivative analysis, the continuous-time observability matrix is obtained as (10) which is shown at the top of the page, where the superscript (i) denotes the ith-order gradient of $g(x)$ to x. More details on the derivation can be found in [26].

As seen from (10), when only the total voltage of every n cells is measured, up to nth order gradients of $g(x)$ need to be checked. In order for the observability matrix to be of full rank (rank $= n$), at least one of each $g^{(i)}(x)$ should be nonzero. Ultimately, the eigenvalues of $O_C(x_{\mathrm{str},k})$ need to be calculated, and full rank requires all the eigenvalues to be nonzero. This part of work is to be addressed in detail in future, and it is foreseeable that reducing voltage sensors further requires stronger nonlinearity on $g(x)$, which could be challenging in practice.

It is noted that the observability will not exist if $g(x)$ is linearized. This is because after linearization, all the higher than second-order gradients become zero, making the rank of $O_C(x_{\mathrm{str},k})$ equal to one. Therefore, it is speculated that the linearization-based estimation approaches cannot be used for SOC estimation under reduced voltage sensing. One of the linearization-based methods is the EKF [14], whose convergence is guaranteed if the linearized plant model is observable [27]. In [26], it is shown by simulation that the estimates of EKF can only track the average SOC of the two-cell string. Furthermore, the observability of cell SOCs cannot be simply concluded based on the rank of the observability. In some cases, for example, when the second-order gradient of $g(x)$ is very small but not strictly zero, the SOCs are not effectively observable although the observability matrix is still of full rank. The singular values and/or the condition number of the observability matrix need to be checked to determine the effective observability of the system. This part will be discussed in details in Section VI-A for different combinations of SOC and capacity imbalance.

V. Newton Observer

Following the observability analysis, a trajectory-based algorithm, the Newton observer [28], [29], will be designed to estimate the individual cell SOC under reduced voltage sensing. The Newton observer is first introduced and then validated by experiments.

A. Design of the Newton Observer

The main idea of the Newton observer is to estimate the states by simultaneously solving multiple nonlinear equations along the output trajectory.

At each estimation step, with the total voltage trajectory $V_{\mathrm{str},[k,k+N]}$ defined in (4), the Newton–Raphson algorithm is applied to estimate $x_{\mathrm{str},k}$ iteratively

$$\hat{x}^{j+1}_{\mathrm{str},k} = \hat{x}^{j}_{\mathrm{str},k} + \left[\frac{\partial H}{\partial x_{\mathrm{str},k}}\left(\hat{x}^{j}_{\mathrm{str},k}\right)\right]^{-1}\left(V_{\mathrm{str},[k,k+N]} - H\left(\hat{x}^{j}_{\mathrm{str},k}\right)\right) \tag{11}$$

where the superscript j denotes the jth iteration, and $\hat{x}_{\mathrm{str},k}$ is the estimate of $x_{\mathrm{str},k}$. Essentially, optimal $\hat{x}_{\mathrm{str},k}$ is searched to minimize the least square error in $V_{\mathrm{str},[k,k+N]}$. The dimension of $\partial H/\partial x_{\mathrm{str},k}$ is $N \times 2$, where N is the number of data points along the voltage trajectory. When $N > 2$, $\partial H/\partial x_{\mathrm{str},k}$ has more rows than columns, and thus its left pseudoinverse should be used

$$\left(\frac{\partial H}{\partial x_{\mathrm{str},k}}\right)^{-1} = \left[\left(\frac{\partial H}{\partial x_{\mathrm{str},k}}\right)^{T}\left(\frac{\partial H}{\partial x_{\mathrm{str},k}}\right)\right]^{-1}\left(\frac{\partial H}{\partial x_{\mathrm{str},k}}\right)^{T}. \tag{12}$$

It is noted that the Newton observer can only be applied when $x_{\mathrm{str},k}$ is observable. The matrix $\partial H/\partial x_{\mathrm{str},k}$ is the discrete-time observability matrix, and its (pseudo)inverse exists if and only if the observability matrix is of full rank as discussed in (7). The convergence of the Newton observer is guaranteed if the nonlinear observability condition is satisfied and the initial guess starts within a certain neighborhood of the actual value [28]. The convergence has been validated by experiments, which will be shown in Section V-B.

After the estimate converges, the individual cell SOCs and voltages at time steps $k+1,\ k+2, \ldots, k+N$ can be determined based on $x_{\mathrm{str},k}$ and the battery string model in (2). At the next estimation step, the measured voltage trajectory is updated with newly acquired data, and becomes $V_{\mathrm{str},[k+W,\,k+W+N]}$, where W is the interval between estimation steps. The initial state at the new estimation step, $x_{\mathrm{str},\,k+W}$, will be estimated based on $V_{\mathrm{str},[k+W,\,k+W+N]}$, and its initial guess is determined based on the final estimate of $x_{\mathrm{str},k}$.

The advantage of the Newton–Raphson algorithm is fast convergence, but the drawback is lack of robustness under certain circumstances. For example, when the SOCs are at the edge of the observable region, $\partial H/\partial x_{\mathrm{str},k}$ is close to rank deficient with a large condition number, posing difficulty to the inversion of $\partial H/\partial x_{\mathrm{str},k}$. To improve the robustness, the Levenberg–Marquardt iteration is used instead [30], [31]

$$\hat{x}^{j+1}_{\mathrm{str},k} = \hat{x}^{j}_{\mathrm{str},k} + \left[\frac{\partial H}{\partial x_{\mathrm{str},k}}\left(\hat{x}^{j}_{\mathrm{str},k}\right) + \alpha \mathbf{I}\right]^{-1} \times \left(V_{\mathrm{str},[k,k+N]} - H\left(\hat{x}^{j}_{\mathrm{str},k}\right)\right) \tag{13}$$

where α is a scalar and $\mathbf{I}$ is a 2×2 identity matrix. The factor $\alpha\mathbf{I}$ is used to lower the condition number and hence stabilize the matrix inversion.

The Newton observer can be generalized to the cases with $n > 2$ as long as the SOCs are observable. In real-time application, computation of the matrix inversion in (12) could be a concern. Dimension of the square matrix $[(\partial H/\partial x_{\mathrm{str},k})^T(\partial H/\partial x_{\mathrm{str},k})]$ is the number of cells, n. The computational load is not an issue for a two-cell string since the inversion of a 2×2 matrix is efficient, but it will be more intense as the number of cells increases.

B. Experimental Validation

The validation of the Newton observer is to be shown based on experiments conducted with two 2.3 Ah $LiFePO_4$ batteries connected in series.

The Coulomb counting model in (1) is first parameterized based on experimental data under 2 Amp CC charging/discharging. This current rate is adjustable according to the power of the charger.

During the validation experiment, the two cells are first initialized with SOCs around $x_{1,0} = 5\%$ and $x_{2,0} = 0\%$. They are then connected in series and charged with a single current source under 2 A CC. Single cell voltages are measured to prevent overcharge and for validation. Actual cell SOCs is calculated based on current integration to validate the SOC estimation. Current is cut off when the voltage of any cell reaches the threshold of 3.6 V. Measured SOCs and voltages are shown in Fig. 5.

The collected voltage and current data are then used for estimation and validation. The initial guess of SOCs for both cells is determined by inverting the average measured voltage. At each estimation step, $V_{\mathrm{str},[k,k+N]}$ contains 15 data points, which are sampled 10-s apart (10 s from k to $k+1$). The time interval W between each estimation step is chosen as 20 s. In this way, SOC estimation is updated every 20 s, corresponding to an SOC increment of 0.5% at 2 A. This rate is sufficient for preventing overcharge in real time.

The estimates of the Newton observer are shown and compared with the measurements in Figs. 6 and 7. The plotted values correspond to the last point at each estimation step. The final estimates are listed in Table II. In Fig. 6, it can be seen that the cell SOCs are not distinguishable since the estimation is equal to the average SOC when both SOCs are below 85%. This observation is in accordance with the observability analysis in Section IV, which predicts that the SOCs are not observable in the middle SOC range due to the nearly linear voltage versus SOC relationship $g(x)$. As the SOCs evolve to the observable range above 90%, the estimates of the Newton Observer converge to the measurement gradually.

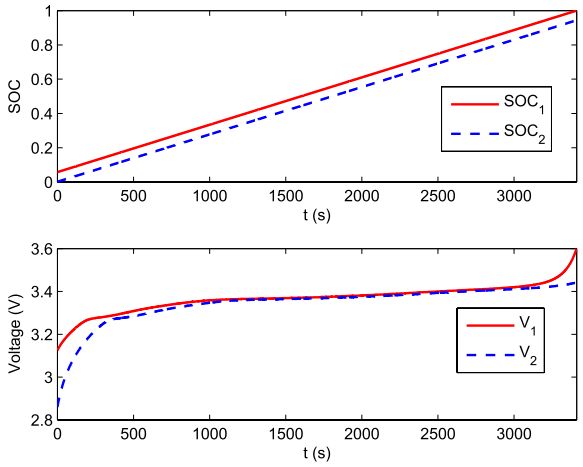

Fig. 5. Measured SOCs and voltages of individual cells under 5% SOC imbalance.

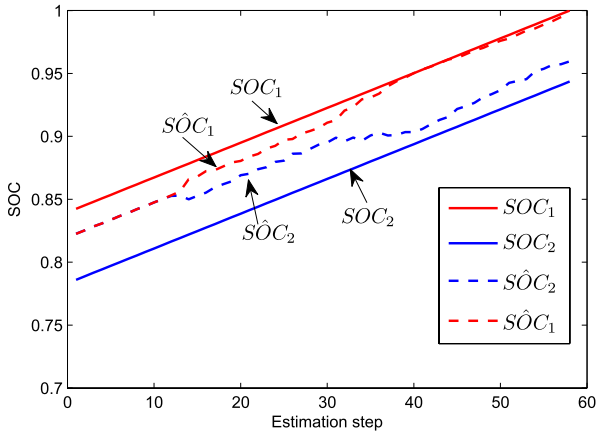

Fig. 6. Comparison of SOC estimation with experiment measurement under 5% SOC imbalance.

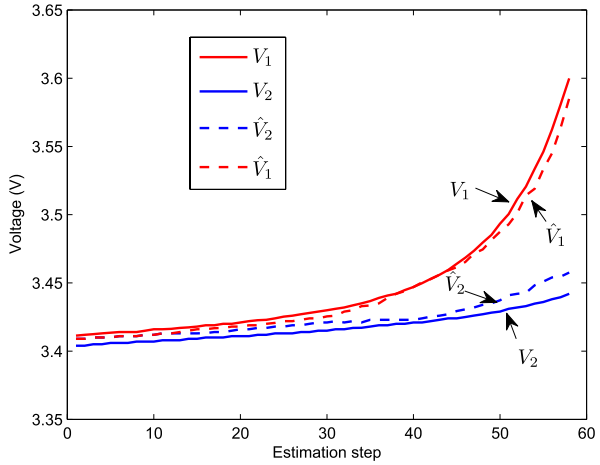

Fig. 7. Comparison of voltage estimation with experiment measurement under 5% SOC imbalance.

TABLE II
FINAL ESTIMATES UNDER 5% SOC IMBALANCE

	Estimates	Measurement	error (%)
SOC_1 (%)	99.81	100	0.19
SOC_2 (%)	95.99	94.36	1.73
V_1 (V)	3.59	3.60	0.28
V_2 (V)	3.46	3.44	0.58

Furthermore, it is noted that the estimate of SOC_1 is more accurate than that of SOC_2. This feature is advantageous for preventing overcharge because cell 1 is closer to being fully charged and hence the precaution is more critical. The reason for the better accuracy of SOC_1 estimation is due to the higher sensitivity of V_{str} to SOC_1, caused by the larger $g'(x)$ at x_1.

VI. SOC ESTIMATION UNDER IMBALANCE IN CAPACITY AND RESISTANCE

For cells connected in series, besides varying self-discharge rate, difference in capacity may also cause SOC imbalance. In this section, the developed methodology will be applied to estimate the individual cell SOCs under imbalance in capacity and resistance. First, the observability of SOCs will be investigated under different combinations of capacity and SOC imbalance. It will be shown that certain combinations inhibit the observability in the original strongly observable high SOC range. The imbalance in resistance is also considered, which does not affect the observability though. Second, the SOC estimation errors will be quantified under uncertainty in capacity and resistance. In the presence of capacity and resistance imbalance, usually only the rated values are known but not the true values of the individual cells. Therefore, SOC estimation based on the Newton observer will be affected by model uncertainty in capacity and resistance. The estimation error will be derived as well as shown in simulation, and its relationship to observability will also be discussed. It is expected that the accuracy of SOC estimation under reduced voltage sensing will deteriorate compared with that under full voltage. The results in this section would demonstrate the performance of the estimation algorithm for a production battery ($LiFePO_4$) under practical uncertainty.

A. Observability of SOCs Under Different Combinations of SOC and Capacity Imbalance

When the capacity and resistance are not equal between the two cells, the true voltage trajectory $V^*_{\text{str},[k,k+N]}$ will be

$$V^*_{\text{str},[k,k+N]} = H\left(x^*_{\text{str},k}, Q^*, R^*\right) = \begin{bmatrix} g\left(x^*_{1,k}\right)+g\left(x^*_{2,k}\right)+I\left(R^*_1+R^*_2\right) \\ g\left(x^*_{1,k}+\frac{I\Delta t}{Q^*_1}\right)+g\left(x^*_{2,k}+\frac{I\Delta t}{Q^*_2}\right)+I\left(R^*_1+R^*_2\right) \\ \cdots \\ g\left(x^*_{1,k}+\frac{NI\Delta t}{Q^*_1}\right)+g\left(x^*_{2,k}+\frac{NI\Delta t}{Q^*_2}\right)+I\left(R^*_1+R^*_2\right) \end{bmatrix}$$
$$Q^* = \begin{bmatrix} Q^*_1 \\ Q^*_2 \end{bmatrix}, \quad R^* = \begin{bmatrix} R^*_1 \\ R^*_2 \end{bmatrix} \tag{14}$$

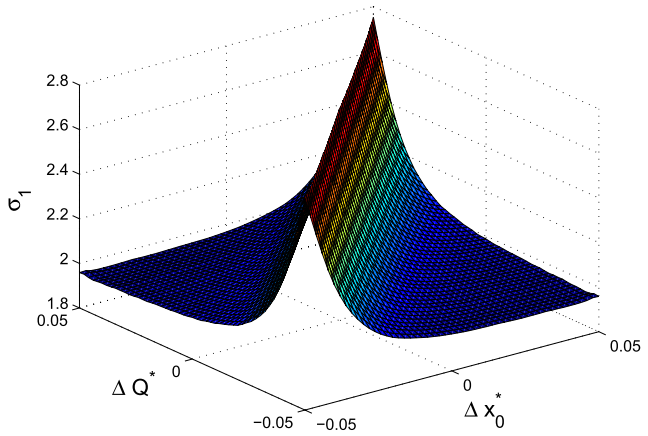

Fig. 8. Singular value σ_1 of the observability matrix O_D at the end of charging.

where the superscript * denotes the true value of the variable. The corresponding discrete observability matrix is derived as

$$O_D\left(x^*_{\text{str},k}\right) = \frac{\partial H}{\partial x_{\text{str},k}}\left(x^*_{\text{str},k}, Q^*\right) = \begin{bmatrix} g'\left(x^*_{1,k}\right) & g'\left(x^*_{2,k}\right) \\ g'\left(x^*_{1,k}+\frac{I\Delta t}{Q^*_1}\right) & g'\left(x^*_{2,k}+\frac{I\Delta t}{Q^*_2}\right) \\ \cdots & \cdots \\ g'\left(x^*_{1,k}+\frac{NI\Delta t}{Q^*_1}\right) & g'\left(x^*_{2,k}+\frac{NI\Delta t}{Q^*_2}\right) \end{bmatrix}. \tag{15}$$

The observability is to be discussed for different combinations of $x^*_{\text{str},k}$ and Q^* based on the singular values of $O_D(x^*_{\text{str},k}, Q^*)$, which quantifies the observability. The capacities Q^*_1 and Q^*_2 are considered as varying between 100% and 95% of the rated capacity Q. In the presence of capacity imbalance, the SOC imbalance will not be constant during battery operation. The initial SOCs are defined with $x^*_{1,0}$ and $x^*_{2,0}$ changing from 0%–5%, respectively. The resulting imbalance in initial SOC and capacity

$$\Delta x^*_0 = x^*_{1,0} - x^*_{2,0}, \quad \Delta Q^*_{\%} = \frac{Q^*_1 - Q^*_2}{Q} \tag{16}$$

will both vary between -5% and $+5\%$. The singular values of O_D, σ_1, and σ_2, are calculated at the last estimation step (the end of charging) for all the combinations, as shown in Figs. 8 and 9.

The smaller singular value σ_2 is the critical one that determines the observability. As seen in Fig. 9, the values of σ_2 for most combinations are above 0.03, except those on the diagonal of the $\Delta x^*_0 - \Delta Q^*$ plane. These combinations have weakly observable SOCs, with condition numbers of O_D $\kappa \geq 99$ as compared with $\kappa < 50$ elsewhere. The existence of these combinations can be deduced from the structure of O_D in (15). If the SOCs of the two cells, at the end of charging, are close to each other, the two columns of O_D will be nearly the same, leading to the large condition number of O_D. Such cases can be represented as

$$x^*_{1,0} + \frac{\int I dt}{Q^*_1} \approx x^*_{2,0} + \frac{\int I dt}{Q^*_2} \quad \Rightarrow \quad x^*_{1,0} - x^*_{2,0} \approx \frac{\int I dt}{Q^*_1}\frac{Q^*_1 - Q^*_2}{Q^*_2} \tag{17}$$

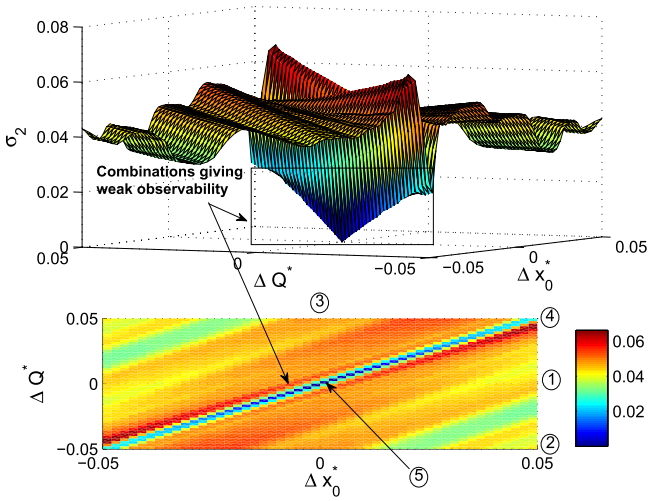

Fig. 9. Singular value σ_2 of the observability matrix O_D at the end of charging. Top plot: values of σ_2 for all combinations. Bottom plot: projection of σ_2 onto the $\Delta x_0^* - \Delta Q^*$ plane.

where $\int Idt$ is the change in stored energy (in amp hour) from the reference point to the end of charging. When the capacity imbalance is within $\pm 5\%$, we have $Q_1^* \approx Q_2^* \approx Q$, giving

$$x_{1,0}^* - x_{2,0}^* \approx \frac{\int Idt}{Q}\frac{Q_1^* - Q_2^*}{Q} \Rightarrow \Delta x_0^* \approx \frac{\int Idt}{Q}\Delta Q_{\%}^*. \quad (18)$$

Since $\int Idt$ is close to the rated capacity Q from the reference point (around 0% SOC) to the end of charging (near 100% SOC), (18) yields

$$\Delta x_0^* \approx \Delta Q_{\%}^*. \quad (19)$$

Consequently, the weakly observable combinations lie along the diagonal of the $\Delta x_0^* - \Delta Q^*$ plane. Nevertheless, it is still possible to achieve an adequate SOC estimation for the weakly observable combinations. For example, by using the singular value decomposition (SVD) method [29], the Newton observer can accurately estimate the strongly observable part of the system. For the weakly observable combinations, it is found in [32] that the strongly observable part is the average SOC of the two cells. Interestingly, since the SOCs of the two cells converge at the end in the weakly observable combinations, the actual SOCs of the two cells are very close to the (strongly observable) average SOC and could therefore be estimated adequately. The Levenberg–Marquardt method applied in this paper could achieve similar performance as the SVD. Details concerning the implementation of SVD can be found in [32].

B. SOC Estimation Error Under Model Uncertainty in Capacity and Resistance

In this section, the error analysis under coupled SOC and capacity/resistance imbalance (and hence uncertainty) is presented and it will be shown how the observability affects the estimation error.

The SOC estimation error will be derived first. In the model-based Newton observer, the capacity and resistance of both cells are assumed to be the rated values Q and R. Modeling errors, δQ and δR, and estimation error in SOC, $e_{x,k}$, are defined as the difference between the true values and the assumed/estimated values

$$\begin{aligned} \delta Q &= \begin{bmatrix}\delta Q_1 \\ \delta Q_2\end{bmatrix} = \begin{bmatrix}Q_1^* - Q_1 \\ Q_2^* - Q_2\end{bmatrix} \\ \delta R &= \begin{bmatrix}\delta R_1 \\ \delta R_2\end{bmatrix} = \begin{bmatrix}R_1^* - R_1 \\ R_2^* - R_2\end{bmatrix} \\ e_{x,k} &= x_{\mathrm{str},k}^* - \hat{x}_{\mathrm{str},k} = \begin{bmatrix}x_{1,k}^* - \hat{x}_{1,k} \\ x_{2,k}^* - \hat{x}_{2,k}\end{bmatrix}. \end{aligned} \quad (20)$$

Based on (14), variation of $V_{\mathrm{str},[k,k+N]}$ under (small) deviation of $x_{\mathrm{str},k}$, Q, and R can be obtained as

$$\delta V_{\mathrm{str},[k,k+N]} = \frac{\partial H}{\partial x_{\mathrm{str},k}}\delta x_{\mathrm{str},k} + \frac{\partial H}{\partial Q}\delta Q + \frac{\partial H}{\partial R}\delta R \quad (21)$$

where $\partial H/\partial x_{\mathrm{str},k}$ is the observability matrix in (15), and

$$\begin{aligned} \frac{\partial H}{\partial Q} &= \begin{bmatrix} 0 & 0 \\ -g'\left(x_{1,k}^* + \frac{I\Delta t}{Q_1^*}\right)\frac{I\Delta t}{(Q_1^*)^2} & -g'\left(x_{2,k}^* + \frac{I\Delta t}{Q_2^*}\right)\frac{I\Delta t}{(Q_2^*)^2} \\ \cdots & \cdots \\ -g'\left(x_{1,k}^* + \frac{NI\Delta t}{Q_1^*}\right)\frac{NI\Delta t}{(Q_1^*)^2} & -g'\left(x_{2,k}^* + \frac{NI\Delta t}{Q_2^*}\right)\frac{NI\Delta t}{(Q_2^*)^2} \end{bmatrix} \\ \frac{\partial H}{\partial R} &= \begin{bmatrix} I & I \\ I & I \\ \cdots & \cdots \\ I & I \end{bmatrix}. \end{aligned} \quad (22)$$

By taking δQ and δR as the modeling uncertainty, $\delta x_{\mathrm{str},k}$ represents the resulting SOC estimation error $e_{x,k}$, and $\delta V_{\mathrm{str},[k,k+N]}$ is the mismatch between the measured and the estimated voltage trajectory. Since the Newton observer estimates $\hat{x}_{\mathrm{str},k}$ by minimizing errors in voltage, $\delta V_{\mathrm{str},[k,k+N]}$ is usually small. Based on (21), with $e_{x,k} = \delta x_{\mathrm{str},k}$, the SOC estimation error $e_{x,k}$ can be quantified as

$$\begin{aligned} e_{x,k} = &\left(\frac{\partial H}{\partial x_{\mathrm{str},k}}\left(x_{\mathrm{str},k}^*, Q^*\right)\right)^{-1} \\ &\times\left[\delta V_{\mathrm{str},[k,k+N]} - \frac{\partial H}{\partial Q}\left(x_{\mathrm{str},k}^*, Q^*\right)\delta Q - \frac{\partial H}{\partial R}\delta R\right]. \end{aligned} \quad (23)$$

For the convenience of comparison, (23) needs to be normalized to the form of percentage error, as

$$\begin{aligned} e_{x,k,\%} = &\left(\frac{\overline{\partial H}}{\partial x_{\mathrm{str},k}}\left(x_{\mathrm{str},k}^*, Q^*\right)\right)^{-1} \\ &\times\left(\delta V_{\mathrm{str},[k,k+N],\%} - \frac{\overline{\partial H}}{\partial Q}\delta Q_{\%} - \frac{\overline{\partial H}}{\partial R}\delta R_{\%}\right) \end{aligned} \quad (24)$$

where

$$\begin{aligned} e_{x,k,\%} &= \begin{bmatrix}\frac{x_{1,k}^* - \hat{x}_{1,k}}{x_{1,k}^*} \\ \frac{x_{2,k}^* - \hat{x}_{2,k}}{x_{2,k}^*}\end{bmatrix} \\ \delta Q_{\%} &= \begin{bmatrix}\frac{Q_1^* - Q_1}{Q_1^*} \\ \frac{Q_2^* - Q_2}{Q_2^*}\end{bmatrix} \\ \delta R_{\%} &= \begin{bmatrix}\frac{R_1^* - R_1}{R_1^*} \\ \frac{R_2^* - R_2}{R_2^*}\end{bmatrix}. \end{aligned} \quad (25)$$

TABLE III
ROBUSTNESS OF SOC ESTIMATION UNDER CERTAIN COMBINATIONS OF IMBALANCE AND DEGRADATION

No.	Initial SOC	Degradation	Q^*	R^*	σ	κ	Predicted $e_{x,\%}$	Simulated $e_{x,\%}$
①	$x_{1,0}=5\%$ $x_{2,0}=0\%$	Cell1: 5% Cell2: 5%	$Q_1^*=0.95Q$ $Q_2^*=0.95Q$	$R_1^*=1.05R$ $R_2^*=1.05R$	1.95 0.045	44	$e_{x,1,\%}=-0.40\%$ $e_{x,2,\%}=1.10\%$	$e_{x,1,\%}=-0.38\%$ $e_{x,2,\%}=1.03\%$
②	$x_{1,0}=5\%$ $x_{2,0}=0\%$	Cell1: 5% Cell2: 0%	$Q_1^*=0.95Q$ $Q_2^*=Q$	$R_1^*=1.05R$ $R_2^*=R$	1.94 0.043	45	$e_{x,1,\%}=-0.3\%$ $e_{x,2,\%}=1.57\%$	$e_{x,1,\%}=-0.27\%$ $e_{x,2,\%}=1.51\%$
③	$x_{1,0}=5\%$ $x_{2,0}=5\%$	Cell1: 5% Cell2: 0%	$Q_1^*=0.95Q$ $Q_2^*=Q$	$R_1^*=1.05R$ $R_2^*=R$	1.95 0.048	41	$e_{x,1,\%}=-0.38\%$ $e_{x,2,\%}=1.07\%$	$e_{x,1,\%}=-0.40\%$ $e_{x,2,\%}=1.30\%$
④	$x_{1,0}=5\%$ $x_{2,0}=0\%$	Cell1: 0% Cell2: 5%	$Q_1^*=Q$ $Q_2^*=0.95Q$	$R_1^*=R$ $R_2^*=1.05R$	2.72 0.028	99	–	$e_{x,1,\%}=-1.05\%$ $e_{x,2,\%}=1.11\%$
⑤	$x_{1,0}=5\%$ $x_{2,0}=5\%$	Cell1: 5% Cell2: 5%	$Q_1^*=0.95Q$ $Q_2^*=0.95Q$	$R_1^*=1.05R$ $R_2^*=1.05R$	2.69 0	∞	–	$e_{x,1,\%}=-1.25\%$ $e_{x,2,\%}=1.91\%$

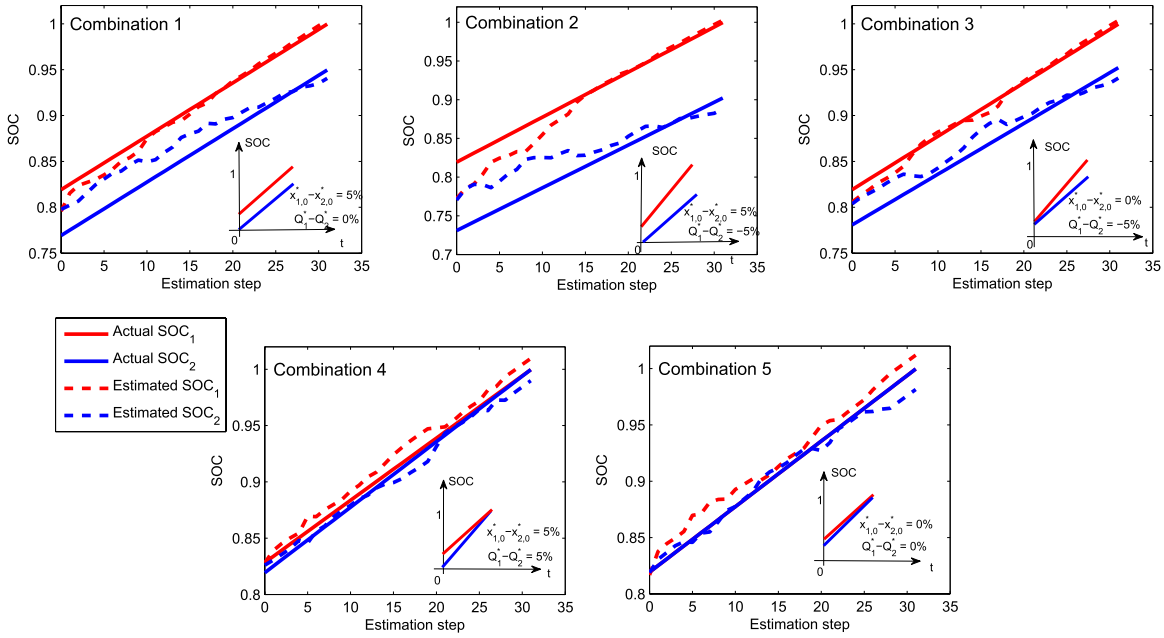

Fig. 10. Simulated SOC estimation under five combinations of SOC imbalance and degradation. The main plots show the estimation results in the high observable SOC range, and the insets show the evolution of actual SOC from 0% to 100%.

The matrices $\overline{\partial H}/\partial x_{\mathrm{str},k}$, $\overline{\partial H}/\partial Q$ and $\overline{\partial H}/\partial R$ are the normalized partial derivatives, and $\delta V_{\mathrm{str},[k,k+N],\%}$ is the normalized voltage trajectory deviation

$$\left[\frac{\overline{\partial H}}{\partial x_{\mathrm{str},k}}\right]_{j,l}=\left[\frac{\partial H}{\partial x_{\mathrm{str},k}}\right]_{j,l}\frac{x_{l,k}^*}{V_{\mathrm{str},k+j-1}^*}$$
$$\left[\frac{\overline{\partial H}}{\partial Q}\right]_{j,l}=\left[\frac{\partial H}{\partial Q}\right]_{j,l}\frac{Q_l^*}{V_{\mathrm{str},k+j-1}^*}$$
$$\left[\frac{\overline{\partial H}}{\partial R}\right]_{j,l}=\left[\frac{\partial H}{\partial R}\right]_{j,l}\frac{R_l^*}{V_{\mathrm{str},k+j-1}^*}$$
$$\left[\delta V_{\mathrm{str},[k,k+N],\%}\right]_j=\frac{\delta V_{\mathrm{str},k+j-1}}{V_{\mathrm{str},k+j-1}^*} \tag{26}$$

where $[\cdot]_{j,l}$ denotes the matrix entry, (j for row index and l for column index). The singular values of O_D, σ, indicate the robustness of the estimation problem [33], [34]. In the presence of model uncertainty, according to (25) where O_D is inverted, the larger the singular values are, the smaller the estimation error $e_{x,k}$ would be.

The SOC estimation under some combinations of SOC and capacity/resistance imbalance is to be discussed as examples. Five combinations are considered, which locate at the labeled spots ①–⑤ on the $\Delta x_0^* - \Delta Q^*$ plane in Fig. 9. The specifications of these combinations are listed in Table III. The imbalance in capacity and resistance is assumed to be caused by differing degree of battery degradation, and the percentage of capacity fade is projected to be the same as that of resistance growth.

The singular values and condition number of the observability matrix, as well as the predicted estimation based on (24) are also listed in Table III. All the values are evaluated at the end of charging (last estimation step when cell 1 is nearly fully charged). Combinations ①–③ are in the strongly observable region, with singular value $\sigma_2 > 0.04$ and condition number $\kappa \leq 50$. Combinations ④ and ⑤, lying on the diagonal of the $\Delta x_0^* - \Delta Q^*$ plane, are weakly observable with $\sigma_2 < 0.03$ and condition number $\kappa \geq 99$. The SOC estimation of the Newton observer for these combinations is simulated using MATLAB/Simulink and shown in Fig. 10. The main plots show the estimation results in the high (observable) SOC range, and the insets show the evolution of actual SOC from 0% to 100%. The initial guess of SOC is determined by inverting the measured average voltage.

It can be seen that the SOC estimation of combinations ①–③ is not greatly affected by the model uncertainty, especially for the critical cell 1, which is fully charged at the end. The SOC estimation errors seen in simulation are very close to the predicted errors based on (24). For combinations ④ and ⑤, the SOCs of the two cells are close to each other at the end of charging, yielding weak observability and hence larger estimation errors. It is noted that although the predicted estimation errors are close to infinity due to the ill-conditioned OD matrix, the actual errors are well bounded (as seen in Table III). The reason is that the Levenberg–Marquardt method applied in the Newton observer is capable of estimating mainly the strongly observable part of the system, and thus reduces the effect of model uncertainty. Still, (more) accurate estimation will require eradication of model uncertainty with better knowledge of capacity and resistance.

VII. Conclusion

In this paper, the problem of estimating battery SOCs under reduced voltage sensing is investigated. It is shown that nonlinearity in the voltage-SOC relationship $g(x)$ is required to render observability to individual cell SOCs from the total voltage. It is also found that the cell SOCs are observable from the trajectory of the total voltage but not from the measurement at a single time instant. Hence, a trajectory-based Newton observer is designed and applied to $LiFePO_4$ batteries, showing good convergence of SOC estimation in the high SOC region where $g(x)$ is highly nonlinear. The solution has been developed and validated under constant current charging condition.

The methodology is initially designed to estimate SOC imbalance due to differing cell self-discharge rates by assuming equal and known capacity and resistance among cells. In reality, due to manufacturing variability and differing degradation rates, imbalance in capacity (and resistance) may exist among cells, which will also lead to SOC imbalance. The methodology is then extended for SOC estimation under different combinations of imbalance in initial SOC and capacity. It is found that for $LiFePO_4$ batteries, the observability in the high SOC range is preserved for most combinations, except for cases where the actual SOC imbalance is very small at the end of charge. For such weakly observable cases, the accuracy of SOC estimation will be affected by model uncertainty in capacity and resistance. To improve the robustness of SOC estimation in these cases, adaptation of capacity and resistance will be addressed in future work. Also as part of the future work, it is desirable to extend the methodology from constant current charging condition to dynamic current input scenario, such as real-world driving. When extended to the complicated driving conditions, the Coulomb counting model is no longer adequate for capturing the battery voltage dynamics. More complicated models need to be used, such as the equivalent circuit model parameterized in [35] and [36]. Ideally, the Newton observer can be built directly upon the new model. Model uncertainty, however, will become a major concern. It is impossible to predict the battery voltage perfectly under dynamic current input with a model, and the mismatch in voltage could be much larger than that under constant current charging. The voltage mismatch will translate into SOC estimation error and thus affect the accuracy of estimation. The robustness of the algorithm is expected to be a major challenge for SOC estimation under dynamic current. The benefit is that it is possible to enhance the observability of the individual cell SOCs through dynamic current input. As shown in (9) and (15), the nonlinear observability matrix depends on the current input. Therefore, the current can be designed to increase the singular values of the observability matrix (or reduce its condition number) to improve the observability by taking advantage of the stationary vehicle charging period of the PHEV or BEV.

Acknowledgment

The authors would like to thank Prof. J. Grizzle, Prof. J. Sun, Prof. J. Freudenberg, Dr. J. Siegel, and S. Mohan from the University of Michigan, Ann Arbor, MI, USA, for their valuable discussion. This work was performed under the Ford/University of Michigan Alliance Project-Battery Cluster-Cell Observability and Control.

References

[1] T. M. Bandhauer, S. Garimella, and T. F. Fuller, "A critical review of thermal issues in lithium-ion batteries," *J. Electrochem. Soc.*, vol. 158, no. 3, pp. R1–R25, 2011.

[2] M. Wakihara, "Recent developments in lithium ion batteries," *Mater. Sci. Eng., R, Rep.*, vol. 33, no. 4, pp. 109–134, 2001.

[3] M. Winter and R. J. Brodd, "What are batteries, fuel cells, and supercapacitors?" *Chem. Rev.*, vol. 104, no. 10, pp. 4245–4270, 2004.

[4] J. McDowall, "Conventional battery technologies-present and future," in *Proc. IEEE Power Eng. Soc. Summer Meeting*, Jul. 2000, pp. 1538–1540.

[5] A. Affanni, A. Bellini, G. Franceschini, P. Guglielmi, and C. Tassoni, "Battery choice and management for new-generation electric vehicles," *IEEE Trans. Ind. Electron.*, vol. 52, no. 5, pp. 1343–1349, Oct. 2005.

[6] S. Hossain, Y. Saleh, and R. Loutfy, "Carbon–carbon composite as anodes for lithium-ion battery systems," *J. Power Sour.*, vol. 96, no. 1, pp. 5–13, 2001.

[7] Y.-S. Lee and M.-W. Cheng, "Intelligent control battery equalization for series connected lithium-ion battery strings," *IEEE Trans. Ind. Electron.*, vol. 52, no. 5, pp. 1297–1307, Oct. 2005.

[8] M. Dubarry, N. Vuillaume, and B. Y. Liaw, "Origins and accommodation of cell variations in Li-ion battery pack modeling," *Int. J. Energy Res.*, vol. 34, no. 2, pp. 216–231, 2010.

[9] W. F. Bentley, "Cell balancing considerations for lithium-ion battery systems," in *Proc. 12th Annu. Battery Conf. Appl. Adv.*, Jan. 1997, pp. 223–226.

[10] J. Vetter *et al.*, "Ageing mechanisms in lithium-ion batteries," *J. Power Sour.*, vol. 147, nos. 1–2, pp. 269–281, 2005.

[11] K. S. Ng, C.-S. Moo, Y.-P. Chen, and Y.-C. Hsieh, "Enhanced Coulomb counting method for estimating state-of-charge and state-of-health of lithium-ion batteries," *Appl. Energy*, vol. 86, no. 9, pp. 1506–1511, 2009.

[12] X. Hu, F. Sun, and Y. Zou, "Estimation of state of charge of a lithium-ion battery pack for electric vehicles using an adaptive Luenberger observer," *Energies*, vol. 3, no. 9, pp. 1586–1603, 2010.

[13] J. Li, J. K. Barillas, C. Guenther, and M. A. Danzer, "A comparative study of state of charge estimation algorithms for $LiFePO_4$ batteries used in electric vehicles," *J. Power Sour.*, vol. 230, pp. 244–250, May 2013.

[14] G. L. Plett, "Extended Kalman filtering for battery management systems of LiPB-based HEV battery packs: Part 3. State and parameter estimation," *J. Power Sour.*, vol. 134, no. 2, pp. 277–292, 2004.

[15] D. Di Domenico, A. Stefanopoulou, and G. Fiengo, "Lithium-ion battery state of charge and critical surface charge estimation using an electrochemical model-based extended Kalman filter," *J. Dyn. Syst., Meas., Control*, vol. 132, no. 6, pp. 061302-1–061313-11, 2010.

[16] F. Sun, X. Hu, Y. Zou, and S. Li, "Adaptive unscented Kalman filtering for state of charge estimation of a lithium-ion battery for electric vehicles," *Energy*, vol. 36, no. 5, pp. 3531–3540, 2011.

[17] I.-S. Kim, "The novel state of charge estimation method for lithium battery using sliding mode observer," *J. Power Sour.*, vol. 163, no. 1, pp. 584–590, 2006.

[18] J. Safi, M. Beeney, M. Kehs, J. Anstrom, S. Brennan, and H. Fathy, "Improving SOC accuracy using collective estimation for lithium ion battery cells in series," in *Proc. Amer. Control Conf.*, Jun. 2014, pp. 254–259.

[19] H. Dai, X. Wei, Z. Sun, J. Wang, and W. Gu, "Online cell SOC estimation of Li-ion battery packs using a dual time-scale Kalman filtering for EV applications," *Appl. Energy*, vol. 95, pp. 227–237, Jul. 2012.

[20] L. Y. Wang, M. P. Polis, G. G. Yin, W. Chen, Y. Fu, and C. C. Mi, "Battery cell identification and SOC estimation using string terminal voltage measurements," *IEEE Trans. Veh. Technol.*, vol. 61, no. 7, pp. 2925–2935, Sep. 2012.

[21] Y. Hu, S. Yurkovich, Y. Guezennec, and B. J. Yurkovich, "Electro-thermal battery model identification for automotive applications," *J. Power Sour.*, vol. 196, no. 1, pp. 449–457, Jan. 2011.

[22] K. A. Smith, C. D. Rahn, and C.-Y. Wang, "Model-based electrochemical estimation and constraint management for pulse operation of lithium ion batteries," *IEEE Trans. Control Syst. Technol.*, vol. 18, no. 3, pp. 654–663, May 2010.

[23] X. Lin, A. G. Stefanopoulou, P. Laskowsky, J. Freudenberg, Y. Li, and R. D. Anderson, "State of charge estimation error due to parameter mismatch in a generalized explicit lithium ion battery model," in *Proc. ASME Dyn. Syst. Control Conf.*, 2011, pp. 393–400, paper DSCC2011-6193.

[24] F. Albertini and D. D'Alessandro, "Observability and forward–backward observability of discrete-time nonlinear systems," *Math. Control, Signals, Syst.*, vol. 15, no. 4, pp. 275–290, 2002.

[25] R. Hermann and A. J. Krener, "Nonlinear controllability and observability," *IEEE Trans. Autom. Control*, vol. 22, no. 5, pp. 728–740, Oct. 1977.

[26] X. Lin, A. G. Stefanopoulou, Y. Li, and R. D. Anderson, "Estimating individual cell SOCs and voltages without single cell voltage measurement," in *Proc. Amer. Control Conf.*, 2013, pp. 704–709.

[27] Y. Song and J. W. Grizzle, "The extended Kalman filter as a local asymptotic observer for discrete-time nonlinear systems," *J. Math. Syst., Estimation, Control*, vol. 5, no. 1, pp. 59–78, 1995.

[28] P. E. Moraal and J. W. Grizzle, "Observer design for nonlinear systems with discrete-time measurements," *IEEE Trans. Autom. Control*, vol. 40, no. 3, pp. 395–404, Mar. 1995.

[29] P. E. Moraal and J. W. Grizzle, "Asymptotic observers for detectable and poorly observable systems," in *Proc. IEEE 34th Conf. Decision Control*, Dec. 1995, pp. 108–114.

[30] K. Levenberg, "A method for the solution of certain non-linear problems in least squares," *Quart. J. Appl. Math.*, vol. 2, no. 2, pp. 164–168, 1944.

[31] D. W. Marquardt, "An algorithm for least-squares estimation of nonlinear parameters," *J. Soc. Ind. Appl. Math.*, vol. 11, no. 2, pp. 431–441, 1963.

[32] X. Lin, "Adaptive estimation of thermal dynamics and charge imbalance in battery strings," Ph.D. dissertation, Dept. Mech. Eng., Univ. Michigan, Ann Arbor, MI, USA, 2014.

[33] B. R. Jayasankar, A. Ben-Zvi, and B. Huang, "Identifiability and estimability study for a dynamic solid oxide fuel cell model," *Comput. Chem. Eng.*, vol. 33, no. 2, pp. 484–492, 2009.

[34] A. P. Schmidt, M. Bitzer, Á. W. Imre, and L. Guzzella, "Experiment-driven electrochemical modeling and systematic parameterization for a lithium-ion battery cell," *J. Power Sour.*, vol. 195, no. 15, pp. 5071–5080, 2010.

[35] X. Lin *et al.*, "A lumped-parameter electro-thermal model for cylindrical batteries," *J. Power Sour.*, vol. 257, pp. 1–11, Jul. 2014.

[36] H. E. Perez, J. B. Siegel, X. Lin, A. G. Stefanopoulou, Y. Ding, and M. P. Castanier, "Parameterization and validation of an integrated electro-thermal cylindrical LFP battery model," in *Proc. ASME Dyn. Syst. Control Conf. (DSCC)*, 2012, pp. 41–50.

Xinfan Lin received the B.S. and M.S. degrees in automotive engineering from Tsinghua University, Beijing, China, in 2007 and 2009, respectively, and the Ph.D. degree in mechanical engineering from the University of Michigan, Ann Arbor, MI, USA, in 2014.

He is currently a Research Engineer with the Department of Vehicle Controls and System Engineering, Research and Advanced Engineering, Ford Motor Company, Dearborn, MI, USA. His current research interests include modeling, model identification, and reduction of battery electrical and thermal dynamics, and model-based observer and controller design for battery management.

Anna G. Stefanopoulou (S'93–M'96–SM'05–F'09) received the Diploma degree in naval architecture and marine engineering from the National Technical University of Athens, Athens, Greece, in 1991, and the Ph.D. degree in electrical engineering and computer science from the University of Michigan, Ann Arbor, MI, USA, in 1996.

She was an Assistant Professor with the University of California at Santa Barbara, Santa Barbara, CA, USA, from 1998 to 2000, and a Technical Specialist with Ford Motor Company, Dearborn, MI, USA, from 1996 to 1997. She is currently a Professor with the University of Michigan, where she is also the Director of the Automotive Research Center, a U.S. Army Center of Excellence in Modeling and Simulation of Ground Vehicles. She has co-authored a book entitled *Control of Fuel Cell Power Systems*, 10 U.S. patents, and 200 publications on estimation and control of internal combustion engines and electrochemical processes, such as fuel cells and batteries.

Dr. Stefanopoulou is a fellow of the American Society of Mechanical Engineers (ASME), the Inaugural Chair of the ASME DSCD Energy Systems Technical Committee, a member of the SAE Dynamic System Modeling Standards Committee, and a member of the U.S. National Research Council Committee on Vehicle Fuel Economy Standards. She received five best paper awards.

Yonghua Li received the Ph.D. degree in control theory and applications from the Beijing University of Aeronautics and Astronautics, Beijing, China.

He has held numerous positions in academia and industry, most recently as a Research Engineer with the Division of Research and Advanced Engineering, Ford Motor Company, Dearborn, MI, USA. He has authored a number of papers and holds several U.S. patents. His current research interests include supervisory control of discrete event systems, automotive engine control, hybrid vehicle control, and automotive traction battery management system.

R. Dyche Anderson received the B.S. degree in chemical engineering from Michigan Technological University, Houghton, MI, USA, and the M.S. degree in chemical engineering from New Mexico State University, Las Cruces, NM, USA.

He is currently a Technical Expert for Battery Controls with Ford Motor Company, Dearborn, MI, USA, where he leads the Advanced Battery Controls and Systems Group, Ford Research and Advanced Engineering. He has 25 years of experience in batteries, battery controls, and battery systems with Ford Motor Company and the Naval Surface Warfare Center, Crane Division, Perry, IN, USA. He has been involved in a wide variety of battery chemistries, including primary, secondary, and reserve systems. He has spent much of his career in product development, having product responsibility in batteries, battery systems, and battery controls, and has delivered batteries, battery controls, and/or battery systems for automotive, missile, and other applications. He has authored or co-authored numerous papers, developed the internal battery controls training course used globally at Ford Motor Company, and holds six patents in battery controls technology.